X Encontro Brasileiro sobre Adsorção
27 a 30 de Abril de 2014
Guarujá - SP

CARBON DIOXIDE-NITROGEN SEPARATION THROUGH DYNAMIC BED MEASUREMENTS FOR CCS PROCESSES.

R. B. Rios; L. S. Correia; G. B. Silva; M. Bastos-Neto; A. E. B. Torres; D. C. S. de Azevedo; C. L. Cavalcante Jr.

1-Grupo de Pesquisa em Separações por Adsorção - GPSA, Departamento de Engenharia Química, Universidade Federal do Ceará - UFC, Campus do Pici s/n, bloco 709, CEP 60455-760, Fortaleza-CE – Brasil
Telefone: (85) 3366-9611 – Fax: (85) 3366-9610 – Email: celio@gpsa.ufc.br

ABSTRACT: The increasing emissions of carbon dioxide have been pointed as a major cause for the global warming, which has been intensifying the greenhouse effect in our planet. Therefore, technologies of Carbon Capture and Storage (CCS) have been developed with the purpose of reducing the concentration of CO_2 in gas emissions (flue gas). Thus, adsorption-based methods are a very promising cost-efficient technology, particularly in processes such as Pressure Swing Adsorption (PSA). The knowledge of adsorption dynamic from in fixed bed is of essential importance for the design of industrial units like PSA. The objective of the present work is to evaluate the suitability of activated carbon (AC) samples for CO_2 capture by measuring multicomponent breakthrough curves. CO_2-N_2 systems have been studied for such purposes and a model based on the Linear Driving Force (LDF) approximation for the mass transfer was developed to simulate these breakthrough curves in the same experimental conditions. The selectivity of the samples for the adsorption of CO_2 over N_2 was also analyzed and compared.

KEYWORDS: carbon dioxide; nitrogen; fixed bed; separation; adsorption; activated carbon.

1. INTRODUCTION

Carbon dioxide has been pointed as a major responsible for the global warming. Its presence in increasing concentrations in the atmosphere has been contributing to increase the greenhouse effect and may be leading to undetermined climate changes (Cavenati *et al*., 2006). Carbon Capture and Storage (CCS) technologies have become a main focus of reducing point-source emissions such as of power plant flue gases (Mulgundmath *et al*., 2012).

The removal of CO_2 from gas emissions has been carried out by means of several technologies, including absorption, cryogenic distillation, membrane separation, and adsorption (Bae *et al*., 2008). Amine based absorption or scrubbing processes have been used for the separation of CO_2 from natural gas and flue gas streams for many years, but despite its large commercial use, this kind of process has several drawbacks, including high energy costs during solvent regeneration, low carbon dioxide loading capacity and high equipment corrosion (Cavenati *et al*., 2006).

Methods based on adsorption using microporous materials are potentially very cost-efficient, particularly in separation systems such as Pressure Swing Adsorption (PSA), which is commonly accepted to be the most attractive, efficient and affordable due to its simple control, low operating and capital investment costs, and higher energy efficiency (Rios *et al*., 2013).

Activated carbons are considered very attractive materials for applications in CO_2 separation from binary mixtures CO_2-N_2 due to their high surface area, micropore volume and suitable pore size distribution. The high availability of carbon sources makes their industrial-scale production relatively more cost-efficient.

A typical post-combustion flue gas emitted from a power plant contains 15-20 mol% CO_2, 5-9% O_2, and the rest N_2 (Adeyemo *et al*., 2010). Therefore, the most important binary system

representative of pre-dried flue gas is CO_2-N_2 mixture (Belmabkhout and Sayari, 2009).

The knowledge of the adsorption equilibrium is of essential importance for the design and optimization of industrial units like PSA and very important for the evaluation of the selectivity and adsorption capacity of adsorbents. However, a more accurate idea of its performance is obtained when performing fixed-bed dynamics experiments with multicomponent mixtures (Grande *et al*., 2013).

This work provides adsorption equilibrium data of pure CO_2 and N_2 on two activated carbons at 298 K and at total pressure of 1.0 MPa, as well as, breakthrough curves of CO_2-N_2 mixtures on the same samples at 298 K and 0.1 MPa. A model using the *Linear Driving Force* (LDF) approximation and considering the energy and momentum balances was applied. The model was validated by comparing simulations with experimental data. The adsorption selectivity for each sample was calculated from the breakthrough curves and from adsorption pure data.

2. MATERIALS AND METHODS

2.1. Experimental Devices

Single gas adsorption equilibria and specific volume of the solid phase were measured gravimetrically with the aid of a magnetic suspension balance (Rubotherm, Germany). Carbon textural properties were obtained by measuring adsorption isotherms of nitrogen at 77 K using an Autosorb-1 MP (Quantachrome, USA).

A dynamic system to obtain breakthrough curves was designed and set up. Its consists of volumetric flow controllers, a back pressure valve, a micrometric valve, a multi-loop valve, a pressure transducer, two gas chromatographs connected in series. This system enables measurements at total pressures from 0.1 to 1.5 MPa, which differentiates it from conventional systems that use chromatography as a method of analysis.

Gas mixtures were prepared by setting the flow of each component with the SideTrak 840 volumetric flow controllers (Sierra Instruments, EUA), with flow range from 0 to 100 mL/min and an accuracy of ± 1% of full scale. The column pressure was measured by a P-30 pressure transducer (WIKA, Germany) with precision ≤0.1%. These pressures were then summed with barometric pressure measurements from a 511 digital manometer (Testo, Germany) with an accuracy of ± 3 mbar and resolution of 0.1 mbar.

A gas chromatograph (Varian, USA) model 450 GC was used to regenerate a stainless steel column of 250 mm length and 4.6 mm internal diameter. The output of the column was connected a multi-loop valve (Valco, USA) with 12 loops of 1 mL each. Each loop was used for collecting and storing, in a pre-determined time of an adsorption experiment, aliquots of CO_2-N_2 mixtures at different compositions in helium (carrier). This multi-loop valve, while capturing an aliquot of the mixture at the outlet of the fixed bed also works as an injector and thus, with the aid of a second gas chromatograph 430 CG model (Varian, USA), it was possible to analyze the composition of the mixture present in each loop. This chromatograph has a thermal conductivity detector (TCD) and a column model 60/90 Carboxen 1000 (Sigma-Aldrich, Canada), specific for CO_2 and N_2. The output flow of the fixed-bed was measured by an ADM 2000 flow meter (HP Agilent, USA) with an accuracy of ± 3% of full scale.

2.2. Pure Adsorption Isotherms

2.2.1. Experimental data: Single-component adsorption isotherms of CO_2 and N_2 were measured on the samples C141 (Carbomafra, Brazil) and WV1050 (MeadWestvaco, USA) in a pressure range of 0-1.0 MPa at 298 K. The activated carbons were pre-treated *in situ* at 423 K under vacuum (1.3×10^{-8} MPa) until no mass variation in the system was observed. Experiments with helium (non-adsorbed gas) were carried out in order to determine the specific volume of the solid phase, enabling the evaluation of the buoyancy effects on measurements with adsorbing gases. Further details of the determination of these adsorption isotherms may be found elsewhere (Bastos-Neto *et al*., 2005).

2.2.2. Adsorption data fit, selectivity and isosteric heat: The parameters for pure-component adsorption were obtained from the Langmuir equation fit to the adsorption isotherm data. The least-squares method with the Levenberg-Marquardt algorithm was applied for the fitting process. The theoretical selectivity ($S_{i\text{-}j}$), defined as the amount adsorbed of pure component *i* in relation to the amount adsorbed of pure component *j* (at the same temperature and pressure), was evaluated by dividing their

respective adsorbed amounts. The isosteric heat of adsorption of the component *i* (ΔH_i) was evaluated from the adsorption isotherms data at three different temperatures (298, 323 and 348 K) for each gas and using the thermodynamic relation reported in Do (1998).

2.3. Breakthrough Curves

2.3.1. Experimental data: Breakthrough curves of CO_2-N_2 were carried out at 0.1 MPa and 298 K for 15% CO_2, 75% N_2 and 10% He molar basis with both adsorbents. Each AC was packed into the same column using the same procedure. The adsorbent bed was pre-treated *in situ* with a helium flow of 12 mL/min under 423 K heating using a forced convection oven. After that, the system was cooled down to 298 K. The time corresponding to the storage of each aliquot was recorded. These loops were analyzed and it was possible to calculate the relationship between the output and feed concentration over time.

2.3.4. Adsorption Selectivity: The selectivity of CO_2 over N_2 was calculated from the results of the breakthrough curves, plotting a graph of molar flow rate of component *i* (F_i) against time and using the following equation:

$$S_{i-j} = \frac{\left[\int_0^{tf_i} \left(F_{i,feed} - F_{i,out}\right)dt\right]}{\left[\int_0^{tf_j} \left(F_{j,feed} - F_{j,out}\right)dt\right]} \frac{C_{g,j}}{C_{g,i}} \qquad (01)$$

2.3.2. Mathematical model: A PSA cycle is a sequential combination of elementary pre-defined steps including co-current pressurization with feed in a fixed bed. A mathematical model used to reproduce this step must consider the phenomena taking place in the gas phase, in the solid phase where adsorption and diffusion take place and the column wall where energy may be transferred to (or from) the surroundings (Ribeiro *et al*., 2008). Material, momentum and energy balance equations (Figure 1) were applied to describe the dynamic behavior of multicomponent adsorption in a fixed bed (Cavenati *et al*., 2006; Ribeiro *et al*., 2008).

The main assumptions and simplifications of this model are: (i) micropore diffusion controls the mass transfer resistance; (ii) the whole system is in thermal equilibrium (column wall, gas and particle has the same temperature); (iii) adsorption equilibrium exists only between gas and solid phases; (iv) the effects of heat axial dispersion were neglected ($\lambda = 0$); (v) adiabatic operation was assumed ($U_g = 0$), since real adsorptive processes operate near to an adiabatic condition due to rapid cycles of operation that do not allow the exchange of heat between the bed and the environment.

In order to solve this model with partial differential equations, boundary and initial conditions are needed. These conditions were used to reproduce co-current pressurization with feed (adsorption step) and are also shown in Figure 1. This mathematical model was implemented in gPROMS environment (Process System Enterprise, UK) and numerically solved using orthogonal collocation on finite elements method (OCFEM).

2.3.3. Model parameters: The gas phase viscosity, μ, was estimated using Wilke's equation (Bird *et al*., 2006). The axial mass dispersion coefficient, D_{ax}, was calculated as described in Lopes *et al*. (2009), using the Equation 2:

$$D_{ax} = (0.45 + 0.55\varepsilon)D_m + 0.35 r_p u_i \qquad (02)$$

where D_m, the molecular diffusivity, was calculated using the Chapman–Enskog equation (Do, 1998), ε is the bed porosity, r_p is the particle radius and u_i is the interstitial velocity. The film heat transfer coefficient between the gas and wall, h_w, was calculated according to Equation 3.

$$h_w = \frac{Nu.k_g}{d_i} \qquad (03)$$

The Nusselt number, *Nu*, was assumed to be 5.77, which corresponds to plug flow with constant wall temperature in a circular tube (Bird *et al*., 2006) and the gas mixture thermal conductivity, k_g, was calculated as reported in Bird *et al*. (2006) at feed conditions and assumed to be constant along the column. The geometric parameters α_w and α_{Wl} were calculated as reported Santos (2001). All other parameters were obtained from Perry *et al*. (1999). The diffusivity in the micropores was estimated using the gPROMS from the comparison between the model and the experimental data.

Mass balance of the fluid phase (0 < z < L):

$$\frac{\partial}{\partial z}\left(\varepsilon D_{ax} C_{g,T}\frac{\partial y_i}{\partial z}\right)-\frac{\partial}{\partial z}\left(uC_{g,i}\right)-\varepsilon\frac{\partial C_{g,i}}{\partial t}-(1-\varepsilon)\left(\varepsilon_P\frac{\partial C_{g,i}}{\partial t}+\rho_{ap}\frac{\partial \bar{q}_i}{\partial t}\right)=0$$

Mass balance of the particle (0 ≤ z ≤ L):

$$\frac{\partial \bar{q}_i}{\partial t}=\frac{\Omega_c D_{c,i}}{r_c^{\,2}}(q_i^{*}-\bar{q}_i)$$

$$q_i^{*}=\frac{q_{\max,i}b_iP_i}{1+\sum_{j=1}^{n}b_jP_j}\ \text{(Extended Langmuir)}$$

Momentum balance (0 ≤ z ≤ L):

$$-\frac{\partial P}{\partial z}=\frac{150\mu(1-\varepsilon)^2}{\varepsilon^3 d_p^{\,2}}u+\frac{1.75(1-\varepsilon)\rho}{\varepsilon^3 d_p}|u|u$$

$$P=C_{g,\mathrm{T}}RT$$

Energy balance of the fluid phase (0 < z < L):

$$\frac{\partial}{\partial z}\left(\lambda\frac{\partial T}{\partial z}\right)-uC_{g,T}Cp_g\frac{\partial T}{\partial z}+\varepsilon RT\frac{\partial C_{g,T}}{\partial t}-4\left(\frac{h_w}{d_i}\right)(T-T_w)+(1-\varepsilon)\varepsilon_p RT_g\frac{\partial C_{g,T}}{\partial t}+\rho_b\sum_{i=1}^{n}(-\Delta H_i)\frac{\partial \bar{q}_i}{\partial t}$$

$$-\left[\varepsilon C_{g,T}Cv_g+(1-\varepsilon)\left(\varepsilon_p\sum_{i=1}^{n}(C_{g,i}Cv_{g,i})+\rho_{ap}\sum_{i=1}^{n}\bar{q}_iCv_{ads,i}+\rho_{ap}Cp_s\right)\right]\frac{\partial T}{\partial t}=0$$

Energy balance of the wall (0 ≤ z ≤ L):

$$\rho_w Cp_w\frac{\partial T_w}{\partial t}=\alpha_w h_w(T-T_w)-\alpha_{wl}U_g(T_w-T_{ref})$$

Boundary conditions for z = 0:

$$u^{inlet}C_{g,i}^{\ inlet}=uC_{g,i}\Big|_{z=0}-\varepsilon D_{ax}C_{g,\mathrm{T}}\Big|_{z=0}\frac{\partial y_i}{\partial z}\Big|_{z=0}$$

$$u^{inlet}C_{g,\mathrm{T}}^{\ inlet}=uC_{g,\mathrm{T}}\Big|_{z=0}$$

$$u^{inlet}C_{g,i}^{\ inlet}Cp_gT_g^{\ inlet}=uC_{g,i}Cp_gT_g\Big|_{z=0}-\lambda\frac{\partial T_g}{\partial z}\Big|_{z=0}$$

Boundary conditions for z = L:

$$\frac{\partial(y_iC_{g,\mathrm{T}})}{\partial z}\Big|_{z=L}=0;\ \frac{\partial u}{\partial z}\Big|_{z=L}=0;\ P\Big|_{z=L}=P^{outlet};\ \frac{\partial T_g}{\partial z}\Big|_{z=L}=0$$

Initial conditions for t = 0:

$$C_{g,T}\Big|_{t=0}=C_{g,helio}^{\ inlet};\ y_{CO2}\Big|_{t=0}=0;\ y_{N2}\Big|_{t=0}=0;\ q_i^{*}\Big|_{t=0}=0;\ T_w=T_g\Big|_{t=0}$$

Figure 1. Mass, momentum and energy balance equations and boundary and initial conditions of the mathematical model of a fixed bed adsorption system.

3. RESULTS AND DISCUSSION

3.1. Adsorbents Characteristics

The textural characteristics of the adsorbent samples are summarized in Table 1. It can be observed that the C141 is essentially microporous, showing a microporosity of around 91% whereas for the WV1050 this value was slightly higher than 53%. The specific volume of the solid phase of C141 and WV1050 measured in the magnetic suspension balance was 0.494 and 0.573 cm^3/g, respectively.

Table 1. Textural characteristics of the adsorbent, obtained from adsorption isotherms of N_2 at 77 K.

Textural characteristics	C141	WV1050
BET surface area [m^2/g]	813	1674
Micropore volume [cm^3/g]	0.43	0.59
Total pore volume [cm^3/g]	0.47	1.10
Average pore width [Å]	14	18

3.2. Adsorption Isotherms

Single component adsorption isotherms of CO_2 and N_2 were measured on C141 and WV1050 at 298 K in the pressure range from 0 to 1.0 MPa and their respective fits were achieved by using the Langmuir equation as shown in Figure 2.

As expected, both activated carbons exhibited preferential adsorption for carbon dioxide in relation to nitrogen over the whole pressure range. At lower pressures, CO_2 isotherm is steeper for the C141 in comparison to the WV1050, which presents lower adsorption capacity until *ca*. 0.58 MPa at 298 K. This means that for use in PSA cycles at moderate pressures (over 0.6 MPa), WV1050 sample is expected to be slightly better than the other activated carbon. Regarding the N_2 isotherms, C141 showed higher adsorbed amount than the WV1050 sample over to the entire analyzed pressure range (up to 1.0 MPa).

Table 2 shows the parameters of the Langmuir equation for each gas and the respective adsorbed amount at 0.1 MPa and 298 K for both adsorbents.

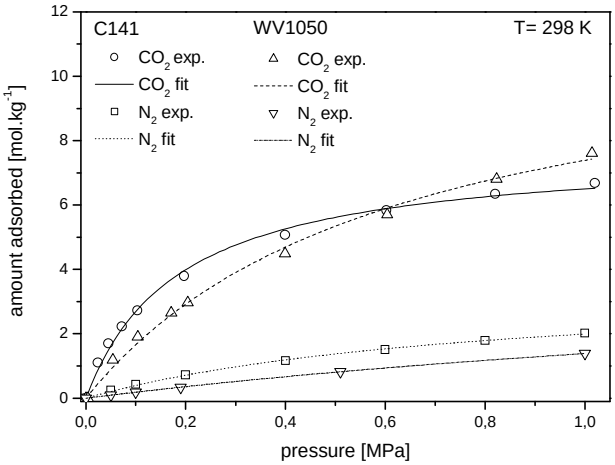

Figure 2. Single component adsorption isotherms of CO_2 and N_2 on the C141 and WV1050 at 298 K. Symbols: Experimental data; Lines: Langmuir fits.

Table 2. Fitting parameters of the Langmuir equation, isosteric heat and amount adsorbed at 0.1 MPa and 298 K.

Adsorption Information	C141		WV1050	
	CO_2	N_2	CO_2	N_2
q_{max} [mol/kg]	7.71	3.61	11.97	4.85
b [MPa^{-1}]	5.36	1.23	1.61	0.40
ΔH [kJ/mol]	25.22	17.68	20.76	16.06
q^* [mol/kg]	2.69	0.43	1.85	0.18

3.3. CO_2-N_2 Breakthrough Curves

Figures 3 and 4 show the breakthrough curves of a CO_2-N_2 mixture in helium (15 mol% CO_2, 75 mol% N_2 and 10 mol% He) at 298 K on C141 and WV1050, respectively.

Even at a concentration of 15 mol%, CO_2 presented higher adsorption capacity with respect to N_2 for both adsorbents, by the analysis of the area under the curve for each gas. This might be explained by the fact that carbon dioxide has a lower critical temperature and therefore it is more likely to behave as a condensable steam rather than as a supercritical gas, becoming less volatile and increasing its surface loading.

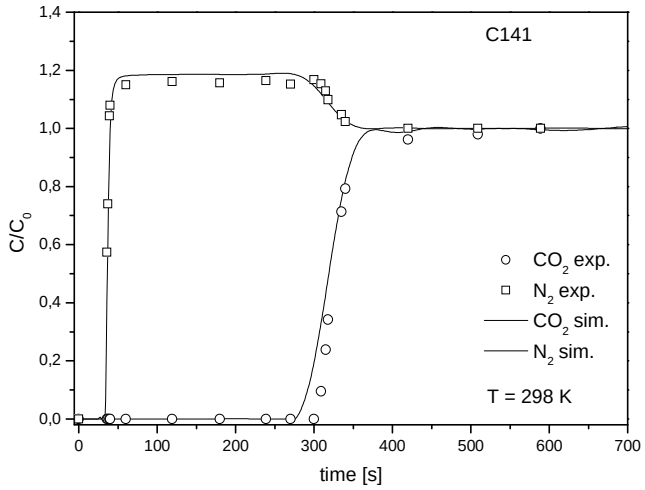

Figure 3. Breakthrough curve of CO_2-N_2 in He (15 mol% CO_2, 75 mol% N_2 and 10 mol% He) at 0.1 MPa and 298 K on C141. Experimental data are symbols and model are the lines.

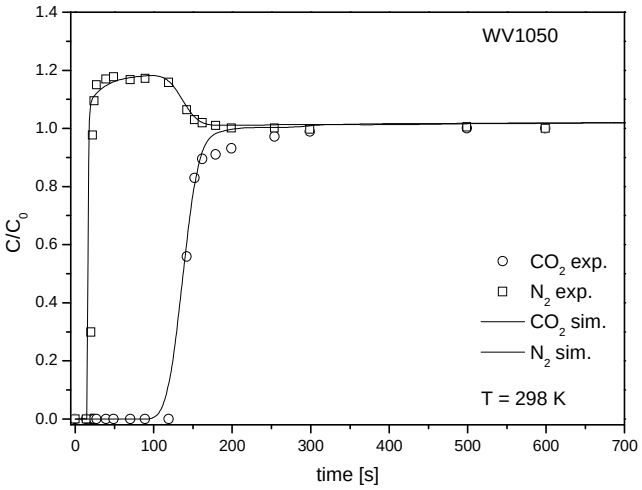

Figure 4. Breakthrough curve of CO_2-N_2 in He (15 mol% CO_2, 75 mol% N_2 and 10 mol% He) at 0.1 MPa and 298 K on WV1050. Experimental data are symbols and model are the lines.

As shown in Table 3, the adsorbent bed had the same size for both materials, but the mass of C141 was about 16% higher than the mass packed of WV1050. From the analysis of Figures 3 and 4, one may also observe that the difference between the bed saturation time of CO_2 in relation to N_2 for C141 was 152% higher than for WV1050. For C141 sample, the difference time was 265 seconds while for WV1050, this difference was approximately 105 seconds, which means that in an industrial application would have more time production of the raffinate (N_2-rich stream) using C141 than the WV1050.

It may be also noticed that the mathematical model reproduces quite well the experimental data even with the considered simplifications. Table 3 shows the main model's parameters used in this work.

Table 3. Model parameters for breakthrough curve simulations at 0.1 MPa and 298 K.

Model Parameters	**C141**	**WV1050**
Bed / column		
L [m]	0.25	0.25
d_i [m]	0.0046	0.0046
ρ_b [kg/m^3]	1065	928
ρ_w [kg/m^3]	7860	7860
α_W [m^{-1}]	929	929
α_{WL} [m^{-1}]	1017	1017
ε	0.474	0.468
Particle		
r_p [m]	4×10^{-4}	4×10^{-4}
ρ_{ap} [kg/m^3]	2026	1745
ε_P	0.486	0.658
k_s	2	2
Momentum		
μ [Pa.s]	1.32×10^{-5}	1.32×10^{-5}
u^{inlet} [m/s]	0.054	0.047
P^{inlet} [MPa]	0.1505	0.1708
Transport		
D_{ax} [m^2/s]	2.824×10^{-5}	2.496×10^{-5}
D_c/r_c^2[s^{-1}]	CO_2: 4×10^{-2} N_2: 2×10^{-2}	CO_2: 4×10^{-2} N_2: 2×10^{-2}
h_w [W/m^2.K]	39.21	39.21
U_q [W/m^2.K]	0	0
λ [W/m.K]	0	0
Energy		
Cp_g [J/mol.K]	34.381	34.381
Cv_g [J/mol.K]	26.121	26.121
Cp_s [J/kg.K]	820	820
Cp_w [J/kg.K]	477	477

Adsorption selectivity gives an idea of the efficiency of the separation. The theoretical selectivities of CO_2-N_2 for each adsorbent at *ca.* 0.1 MPa and 298 K were compared to the

selectivity at same conditions calculated from the breakthrough curves and are shown in Table 4.

Table 4. Selectivity of CO_2-N_2 at 0.1 MPa and 298 K on C141 and WV1050.

Selectivity CO_2-N_2	**C141**	**WV1050**
theoretical	6.26	10.28
breakthrough	8.83	8.57

As the theoretical selectivity does not take into account the competition of components by adsorption sites, their values are quite different from a selectivity calculated from multicomponent data. The analysis of the selectivity at 0.1 MPA and 298 K estimated from column dynamics data (showed in this work), suggests that the C141 sample has a greater potential for the separation of CO_2 from N_2, which was also inferred from the different retention times. For post-combustion scenarios, we should evaluate the selectivity at temperatures close to that found in these processes, which will be studied in future works.

4. CONCLUSIONS

The dynamic adsorption of CO_2-N_2 was evaluated at 298 K on activated carbons from breakthrough curves, as well as the single-component adsorption capacity of CO_2 and N_2 at 298 K from gravimetric measurements. A LDF model was implemented to reproduce these multicomponent data. The adsorption selectivity of CO_2 over N_2 was evaluated without taking into account the co-adsorption effects of CO_2 and N_2 and then compared with the selectivity estimated from multicomponent breakthrough curves. The results show that C141 has selectivity CO_2-N_2 about 8.8, slightly higher than the value for WV1050. The model could satisfactorily predict such dynamic behavior taking into account only micropore resistance and therefore it might be used to verify other scenarios of composition and operating conditions.

5. NOMENCLATURE

b_i Langmuir parameter, Pa^{-1}

$C_{g,i}$ gas phase concentration of component *i*, mol/m^3

$C_{g,T}$ total gas phase concentration, mol/m^3

Cp_g gas mixture molar specific heat at constant pressure, J/mol.K

Cp_s particle specific heat at constant pressure (per mass unit), J/kg.K

Cp_w wall specific heat at constant pressure (per mass unit), J/kg.K

$Cv_{ads,i}$ molar specific heat of component *i* in the adsorbed phase at constant volume, J/mol.K

Cv_g gas mixture molar specific heat at constant volume, J/mol.K

$Cv_{g,i}$ molar specific heat of component *i* at constant volume, J/mol.K

D_{ax} axial dispersion coefficient, m^2/s

$D_{c,i}$ micropore diffusivity of component *i*, m^2/s

d_i internal bed diameter, m

d_p particle diameter, m

h_w film heat transfer coefficient between the gas and wall, $J/s.m^2.K$

ΔH_i heat of adsorption of component *i*, J/mol

k_s geometrical factor (0-slab; 1-cylinder; 2-sphere), dimensionless

P bulk gas mixture pressure, Pa

P_i partial pressure of component *i*, Pa

q_i^* adsorbed concentration in equilibrium with $C_{g,i}$, mol/kg

$\bar{q}_i$ particle averaged adsorbed concentration, mol/kg

$q_{\max,i}$ specific saturation adsorption capacity in the Langmuir isotherm, mol/kg

R ideal gas constant, J/mol.K

r_c "microparticle" radius, m

t time, s

T bulk phase temperature, K

T_{ref} ambient temperature, K

T_w wall temperature, K

u superficial velocity, m/s

U_g overall heat transfer coefficient, $J/s.m^2.K$

y_i component *i* molar fraction, dimensionless

z axial position, m

Greek letters

α_w ratio of the internal surface area to the volume of the column wall, m^{-1}

α_{wl}	ratio of the log mean surface to the volume of column wall, m^{-1}
ε	bed porosity, dimensionless
ε_P	particle porosity, dimensionless
λ	heat axial dispersion coefficient, J/s.m.K
μ	bulk gas mixture viscosity, Pa.s
ρ	bulk gas mixture density, kg/m^3
ρ_{ap}	apparent particle density, kg/m^3
ρ_b	bed density, kg/m^3
ρ_w	wall density, kg/m^3
Ω_c	LDF factor [$\Omega_c = (k_s + 1)(k_s + 3)$], dimensionless

6. REFERENCES

ADEYEMO, A.; KUMAR, R.; LINGA, P.; RIPMEESTER, J.; ENGLEZOS, P. Capture of carbon dioxide from flue or fuel gas mixtures by clathrate crystallization in a silica gel column. *Int. J. Green. Gas Con.*, v. 4, p. 478, 2010.

BAE, Y.; MULFORT, K.L.; FROST, H.; RYAN, P.; PUNNATHANAM, S.; BROADBELT, L.J.; HUPP, J.T.; SNURR, R.Q. Separation of CO_2 from CH_4 Using Mixed-Ligand Metal-Organic Frameworks. *Langmuir*, v. 24, p. 8592-8598, 2008.

BASTOS-NETO, M.; TORRES, A. E. B.; AZEVEDO, D. C. S.; CAVALCANTE JR., C. L. Methane adsorption storage using microporous carbons obtained from coconut shells. *Adsorption*, v. 11, p. 911-915, 2005.

BELMABKHOUT, Y.; SAYARI, A. Adsorption of CO_2 from Dry Gases on MCM-41 Silica at Ambient Temperature and High Pressure. 2: Adsorption of CO_2/N_2, CO_2/CH_4 and CO_2/H_2 Binary Mixtures. *Chem. Eng. Sci.*, v. 64, p. 3729-3735, 2009.

BIRD, R.B., STEWART, W.E.; LIGHTFOOT, E. N. Transport Phenomena, revised second ed., *Wiley International*, New York, 2006.

CAVENATI, S.; GRANDE, C. A.; RODRIGUES, A. E. Separation of $CH_4/CO_2/N_2$ mixtures by layered pressure swing adsorption for upgrade of natural gas. *Chem. Eng. Sci.*, v. 61, p. 3893, 2006.

DO, D. D. Adsorption Analysis: Equilibria and Kinetics. Series on Chemical Engineering, v. 2, *Imperial College Press*, London, 1998.

GRANDE, C. A.; BLOM, R.; MÖLLER, A.; MÖLLMER, J. High-pressure separation of CH4/CO2 using activated carbon. *Chem. Eng. Sci.*, v. 89, p. 10-20, 2013.

LOPES, F. V. S.; GRANDE, C. A.; RIBEIRO, A. M.; LOUREIRO, J. M.; EVAGGELOS, O.; NIKOLAKIS, V.; RODRÍGUES, A. E. Adsorption of H_2, CO_2, CH_4, CO, N_2 and H_2O in activated carbon and zeolite for hydrogen production. *Sep. Sci. Technol*., v. 44, p. 1045-1073, 2009.

PERRY, R. H.; GREEN, D. W.; MALONEY, J. O. Perry's Chemical Engineers' Handbook, 7th ed., *McGraw-Hill*, New York, 1999.

RIBEIRO, A. M.; GRANDE, C. A.; LOPES, F. V. S.; LOUREIRO, J. M.; RODRÍGUES, A. E. A parametric study of layered bed PSA for hydrogen purification. *Chem. Eng. Sci.*, v. 63, p. 5258-5273, 2008.

RIOS, R. B.; STRAGLIOTTO, F. M.; PEIXOTO, H. R.; TORRES, A. E. B.; BASTOS-NETO, M.; AZEVEDO, D. C. S.; CAVALCANTE JR., C. L. Studies on the adsorption behavior of CO_2-CH_4 mixtures using activated carbon. *Braz. J. Chem. Eng.*, v. 30, 4, p. 939-951, 2013.

SANTOS, M. P. S. Advanced modeling of PSA processes for biogas upgrading. *Master Thesis*, University of Porto, 2011.